AN EFFICIENT METHOD FOR COMPUTING UNSTEADY TRANSONIC AERODYNAMICS OF SWEPT WINGS WITH CONTROL SURFACES

D. D. Liu[*] and Y. F. Kao[†]
Department of Mechanical and Aerospace Engineering
Arizona State University
Tempe, Arizona

and

K. Y. Fung[*]
Department of Aerospace and Mechanical Engineering
University of Arizona
Tucson, Arizona,.

ABSTRACT [#]

A transonic equivalent strip (TES) method has been further developed for unsteady flow computations of arbitrary wing planforms. The TES method consists of two consecutive correction steps to a given nonlinear code such as LTRAN2; namely, the chordwise mean-flow correction and the spanwise phase correction. The computation procedure requires direct pressure input from other computed or measured data. Otherwise, it does not require airfoil shape or grid-generation for given planforms. To validate the computed results, four swept, tapered wings of various aspect ratios, including those with control surfaces, are selected as computational examples. Overall trends in unsteady pressures are established with those obtained by XTRAN3S codes, Isogai's full potential code and measured data by NLR and RAE. In comparison with these methods, the TES has achieved considerable saving in computer time and reasonable accuracy which suggests immediate industrial applications.

INTRODUCTION

Considerable attention has been directed in recent years towards the technology development of transonic aeroelastic applications with particular emphasis on transonic flutter predictions. Based on transonic small-disturbance equations (TSDE), computational methods for unsteady transonic flow have been developed extensively both in two and three dimensions, notably LTRAN2 (now ATRAN2) (Refs. 1,2) and XTRAN3S computer codes. Various versions of XTRAN3S codes (Refs. 3,4,5) and a number of full potential methods (Refs. 6,7) are all in good progress. Recently, Guruswamy and Goorjian (Ref. 3), and Borland and Sotomayer (Refs. 4,8) have applied their XTRAN3S codes to Northrop F-5 wing planform. Bennett et al. (Ref. 9) have applied Langley XTRAN3S code for a RAE swept wing; Ruo and Malone (Ref. 10) have applied the same code for LANN wing computations. Isogai and Suetsugu (Ref. 6) have applied their full potential code to various planforms including the AGARD standard RAE wing with an oscillating flap. Most of these results have shown good agreement with the measured data of NLR and RAE.

Although these methods could produce reasonably accurate results, computation efficiency and the grid generation procedures remain to be improved before these codes can be adopted for industrial applications. For flutter predictions and aeroelastic optimizations, a more efficient computer code capable of rapid computations is sought by the aerospace industries, since cost-effectiveness is one of their main concerns.

Motivated by these considerations, we have set forth to develop a simple and more efficient method for unsteady, three-dimensional flow computations. Our objective is to achieve: (1) computation efficiency, (2) flexibility and ease of applications for flutter and (3) a unified subsonic/transonic method for arbitrary planforms. Consequently, a preliminary version of the transonic equivalent strip (TES) method has been developed (Ref. 11). The results obtained for rectangular-wing studies show promise for the TES formulation. Hence, it prompts further development. In this paper, the TES method is further developed so that all procedures are automated for aerodynamic computations. Thus it can be readily adopted by the flutter prediction and the aeroelastic optimization programs. To validate the present method, a fairly comprehensive comparison with available data is given for a number of wing planforms including those with control surfaces.

TRANSONIC EQUIVALENT STRIP (TES) METHOD

The use of strip concept for unsteady transonic computations was first proposed by the ONERA group (Ref. 12). A similar strip approach, but involving quasi-steady approximations, was recently implemented at NLR (Ref. 13). In both cases, however, only wing planforms of large aspect-ratio are treated and possible applications of their methods to low aspect-ratio wings are not forthcoming. By contrast, the present TES method has developed a more general scheme which could handle arbitrary planforms including oscillating control surfaces.

Correction Procedures

Specifically, the present method consists of the applications of two correction steps to a given two dimensional code; it could be a nonlinear code such as LTRAN2 or it could be a time linearized one. The basic correction steps are: (1) the mean-flow correction applied in the chordwise direction and (2) the phase correction in the spanwise direction (see Fig. 1 for flow chart). The first correction is fully automated by an inverse design procedure (IAF2 code) in that the local shock structure is properly recovered according to the given mean flow input provided by a selected computational method or by measured data. In this inverse problem, as solved by Fung and Chung (Ref. 14), the velocity

[†]Associate Professor, Member AIAA
[†]Graduate Student

[#]Also published as AIAA-85-4058.

potential from integrating the pressure on the slit representing an airfoil is known up to an arbitrary constant. To determine this constant, a closure condition is imposed, e.g., the resulting slope distribution being equivalent to a closed body. This constant is being updated during the numerical iteration process until a converged solution satisfying the closure requirement is obtained. Once the slope distribution of the new equivalent airfoil is found and the steady flow field fixed, unsteady responses can then be calculated by varying the slopes to account for unsteady motions. The latter step can be accomplished by applying LTRAN2 code to the equivalent airfoil.

For the second correction, we make use of the three-dimensional linear wave analogy in the sense that the phase angles are redistributed along the span according to the physical model of acoustic wave propagations in a uniform medium. This is to say that while the first correction accounts for reproducing the nonlinear structure of the three-dimensional mean flow, the second correction is responsible for the adjustment of the spanwise phase lag of the pressure according to an equivalent linear three-dimensional flow. In practice, a typical lifting surface method such as Doublet Lattice code (Ref. 15) is adopted for the second correction. Clearly, shock waves cannot be created or destroyed by any process of these corrections.

We should note that the present terminology of "strip method" is defined only by the stripwise computation procedure and is otherwise irrelevant to the classical strip theory. The above correction procedures clearly indicate that the present TES approach is equivalently three-dimensional, since there is no restriction to the wing aspect-ratio.

Justification

It has been pointed out by Fung and Lambourne (Ref. 16,17), among others, that an accurate steady state with correct shock jump and location is essential for correct unsteady aerodynamic computations. It is believed that TSDE in general should be adequate for computation of unsteady disturbances, which are acoustic signals assumed to be small in conventional flutter analysis. However, when applying TSDE methods, inaccuracy may occur as a result of the local failure at the wing leading edge and the limitation in the prediction of the shock strength. Since an accurate steady state pressure field is desired, an alternative is to find the airfoil slopes, or equivalently the airfoil, that corresponds to a given pressure distribution. This, in turn, suggests the inverse design procedure used in the first correction.

Meanwhile, the unsteady aerodynamics of wing flutter at transonic speed is complicated by the embedded supersonic region. Disturbances downstream cannot be felt directly at an upstream point. As a result, the phase lag between unsteady motion of the wing and corresponding aerodynamic response increases as the supersonic region gets larger. While this effect is important in the chordwise direction of a wing, the existence of supersonic region should not affect the way an acoustic signal propagates in the spanwise direction. With the exception of highly-swept wings, the flow-induction effect in the spanwise direction should be subsonic in nature. It is therefore conceivable that the correlation between the aerodynamic responses at different spanwise stations is a linear one as assumed in conventional flutter analysis, and that the unsteady aerodynamic responses due to structural deformations of a wing at transonic speeds are

similar in nature to those at the corresponding subsonic speeds, except in the streamwise direction.

ANALYSIS

Governing Equations

The simplest form of the time-dependent three-dimensional TSDE can be expressed as

$$C\phi_{xx} + D\phi_{yy} + \phi_{zz} = 2B\phi_{xt} + A\phi_{tt} , \qquad (1)$$

where

$$A = M_\infty^2 k^2/\delta^{2/3} , \quad B = M_\infty^2 k/\delta^{2/3}, \quad C = K - \Gamma\phi_x,$$

$$K = (1-M_\infty^2)/\delta^{2/3}, \quad \Gamma = (\gamma+1)M_\infty^2 \quad \text{and}$$

$$D = c^2/b^2\delta^{2/3}.$$

The nondimensional quantities and coordinates are defined as

$$\phi = \bar{\phi}/(c\delta^{2/3}U_\infty) ,$$

$$(x,y,z) = (\bar{x}/c, \bar{y}/b, \bar{z}\delta^{1/3}/c),$$

$$t = \bar{t}\omega \quad \text{and} \quad k = \omega c/U_\infty ,$$

where all barred symbols denote the true physical quantities, parameters c, b, δ and ω represent the root chord, the semi-span, the airfoil thickness ratio and the circular frequency of oscillation, respectively.

The potential ϕ can be split into two components, i.e.,

$$\phi = \phi_0(x,z,t) + \phi_1(x,y,z,t;\Delta\alpha) \qquad (2)$$

where ϕ_0 satisfies the nonlinear, two-dimensional equation (set D = 0 in Eq. (1)) as can be solved by LTRAN2 code; ϕ_1 is the correction potential accounting for the three-dimensional effect attributed to a small unsteady disturbance due to the amplitude $\Delta\alpha$. The three-dimensional unsteady disturbance is assumed to be small as compared to the two-dimensional one at all times; hence, the nonlinear term in the ϕ_1-equation can be neglected, resulting in a linear equation for ϕ_1, i.e.

$$K\phi_{1xx} - \Gamma(\phi_{0x}\phi_{1x})_x + D\phi_{1yy} + \phi_{1zz} = 2B\phi_{1xt} + A\phi_{1tt} \qquad (3)$$

Foregoing physical argument in the TES method allows for further simplification of Eq. (3) by ignoring the coupling term $(\phi_{0x}\phi_{1x})_x$. In so doing, Eq. (3) is reduced to the acoustic equation, where ϕ_1 can be simply solved by the conventional subsonic lifting surface method (Ref. 15).

To further justify the spanwise connection procedure, it is helpful to investigate the characteristic surfaces due to Eq. (1),

$$(x-\frac{B}{A}t)^2 + (C+\frac{B^2}{A})z^2 + (\frac{C}{D} + \frac{B^2}{AD})y^2 = (\frac{B^2}{A^2} + \frac{C}{A})t^2 \qquad (4)$$

Expressed in the dimensional form and for t > 0, Eq. (4) can be recast into a general form, see Fig. 2A

$$(\bar{x} - U_\infty\bar{t})^2 + (\lambda\bar{y})^2 + (\lambda\bar{z})^2 = (\lambda a_\infty\bar{t})^2 \qquad (5)$$

where $\lambda^2 = 1$, for linearized subsonic flow,

$\lambda^2 = 1-(\gamma+1)M_\infty M_\ell$, for transonic flow.

141

M_ℓ is a local, small-disturbance Mach number, defined as $M_\ell = \phi_x / a_\infty$; hence, λ^2 must be positive or zero. Eq. (5) indicates that the traveling source of small disturbance is emitted from $(U_\infty t, 0, 0)$ at the instant t, whose wave front is a sphere for linearized subsonic flow and an ellipsoid for transonic flow (Fig. 2A). Hence, the expanding wave fronts propagate at wave speeds in the chordwise- and spanwise-strip planes, for $y = y_i$ and $x = x_i$, respectively, with

$$\frac{d\bar{R}}{dt} = \frac{a_\infty^2 \bar{t}}{\sqrt{a_\infty^2 \bar{t}^2 - \bar{y}_i^2}} \qquad \text{(chordwise)}$$

and

$$\frac{d\bar{R}}{dt} = \frac{(a_\infty^2 - U_\infty^2)\bar{t} + U_\infty \bar{x}_i}{\sqrt{a_\infty^2 \bar{t}^2 - (\bar{x}_i - U_\infty \bar{t})^2}} \qquad \text{(spanwise)}$$

Note that at $x_i = U_\infty t$ or $y_i = 0$, the rate of propagation becomes identically sonic; otherwise it is time-dependent. Most importantly, along these strip planes, the event diagrams (x-t diagrams) clearly show that while the propagation in the chordwise strip plane is of mixed type which could be either locally subsonic or supersonic, depending on the difference between a_∞ and U_∞, the propagation in the spanwise strip is unconditionally subsonic, which is independent of the a_∞ and U_∞ relations (Fig. 2B).

Boundary Conditions

On the mean surface of the wing planform the potentials must satisfy the tangency condition, i.e. at $z = 0$,

$$\phi_{0_z} = \delta F_x(x, y_i) + \alpha_0 + \alpha_1 \cdot (H_x + kH_t) , \qquad (6)$$

$$\phi_{1_z} = \Delta\alpha \cdot (H_x + kH_t) , \qquad (7)$$

where $F(x, y_i)$ is the stripwise wing surface geometry, y_i is the "ith" spanwise location, α_0 is the mean angle of attack, and $H(x, t)$ depicts the wing motion with oscillation amplitude $\alpha_1 + \Delta\alpha$. While $\Delta\alpha$ is the small amplitude which induces the three-dimensional unsteady disturbances, $\Delta\alpha$ is actually related to the two-dimensional amplitude α_1 by $\Delta\alpha = o(\alpha_1)$.

Outside of the wing planform, the potential ϕ must satisfy the radiation condition in the lateral and the upstream far fields. The zero pressure jump condition across the wake sheet and along which there is no flow discontinuity must be maintained. Also, an unsteady pressure wave must attenuate far downstream. Since these boundary conditions are linearized consistent with the small-disturbance assumption, expressions for ϕ_0 and ϕ_1 become decoupled. Thus, it renders the correction steps to be applied in a consecutive manner.

Pressure Coefficients

Due to a small oscillatory amplitude α, the pressure coefficient can be decomposed into

$$\bar{c}_p = c_p + \Delta c_p \cdot \alpha$$

where c_p is the steady mean pressure coefficient and Δc_p is the unsteady pressure coefficient defined as

$$\Delta c_p^j = \left(\frac{p_u^j - p_\ell^j}{\frac{1}{2}\rho_\infty U_\infty^2}\right) / \alpha^j \qquad (8)$$

with P_u and P_ℓ denoting the pressure at upper and lower surfaces, the superscript $j = \ell$, N and "ℓ" denotes the linear subsonic values and "N" denotes the nonlinear transonic values. Clearly,

$$\alpha^N = \alpha_1 \quad \text{and} \quad \alpha^\ell = \Delta\alpha .$$

In terms of the strip concept, Eq. (6) can be written as

$$\Delta c_{p_1}^j = c_1 \, p_1^j \, (x, y, z; k) , \qquad (9)$$

$$\Delta c_{p_0}^j = c_0 \, p_0^j \, (x, y_i, z; k) , \qquad (10)$$

where c_1 and c_0 are constants and the subscripts 0 and 1 denote, respectively, the two-dimensional strip value and the three-dimensional value at the spanwise location $y = y_i$. While the first correction is applied at the level of Eq. (8), the spanwise correction is implied by the pressure-mode relation between p_1^j and p_0^j which can be expressed as

$$p_1^j = p_0^j \, f^j(y; k) . \qquad (11)$$

According to the foregoing arguments of wave propagations in the stripwise characteristic plane, the nonlinear spanwise pressure function $f^N(y; k)$ can be approximated by its linear counterpart $f^\ell(y; k)$ throughout the spanwise correction procedure.

In passing, we note that in all the figures presented, $\Delta c_p'$ and $\Delta c_p''$ are the real and imaginary parts of the unsteady pressure Δc_p representing the in-phase and out-of-phase pressure coefficients.

RESULTS AND DISCUSSION

To demonstrate the present TES method and to validate its computed results, four different wing planforms are selected for comparison with available data. These include Northrop F-5 Wing in pitching motion and with an oscillating flap, LANN wing in pitching motion, RAE/AGARD tailplane in pitching motion and AGARD standard RAE wing with an oscillating flap. The sections selected are given in the table 1 below:

Table 1 Selected Wing Sections

Planforms	Sections	/	Semi-Span %
F-5 Wing	1, 2, 3, 5,	/	18.1, 35.2, 51.2, 72.1,
	6, 7, 8	/	81.7, 87.5, 97.7
LANN Wing	2, 3, 4,	/	32.5, 47.5, 65.0
	5, 6	/	82.5, 95.0
RAE Tailplane	1, 2, 3, 5	/	14.0, 42.0, 66.0, 96.0

Steady Mean-Flow Results: Equivalent Airfoil Design

For all steady mean-flow pressure design outputs, the present computed results using the IAF2 code for equivalent airfoil design are shown by solid lines, whereas the input data in general are

142

shown by open symbols. Figure 3A and 3B display the pressure inputs for upper and lower surfaces at selected sections listed above at $M_\infty = 0.9$ for LANN wing and F-5 wing based on NLR's measured data (Refs. 18,19). For the case of F-5 wing at $M_\infty = 0.95$, it can be seen from Figure 3C that "strong" shock occurs near the wing trailing edge. Hence some care must be exercised to input the pressure data. To demonstrate the flexibility of the TES method, we adopt the computed results of XTRAN3S-Ames (Ref. 3) as our pressure inputs. Notice that minor discrepancies between input and output results appear behind the mean shock. Figure 10A shows the comparison of input data measured by RAE (Ref. 9) and the TES output results for a RAE tailplane at $M_\infty = 0.9$. Figure 11 presents the steady pressures for the RAE wing at 45% spanwise location using the computed results of the Bailey-Ballhaus code (or GACBOPPE code) as inputs, as no measured data were provided for this section in Ref. 20. For all cases considered, the comparison between the input data and the output computed results are generally in good agreement.

Unsteady Pressure Results: LTRAN2/TES Computations

For unsteady computations, the LTRAN2 code is adopted as our computation basis because of its inclusion of nonlinearity and ease of application. In all figures presented for unsteady pressures, solid lines denote the present TES method, whereas lines attached with triangular symbols represent various versions of XTRAN3S codes, with the exception of Figure 11. The open square and circle symbols denote the NLR or RAE measured data for in-phase and out-of-phase pressures, respectively.

Figures 4, 5 and 6 contain unsteady results at various spanwise sections of Northrop F-5 wing in pitching oscillation at $M_\infty = 0.9$ and at given reduced frequencies $k_c = 0.274$, 0.55 and 0.136, respectively. Figure 7 presents the unsteady results for the same wing in pitching oscillation at $M_\infty = 0.95$. The pitching axes for all cases of F-5 wing are located at 50% root chord. For all cases at $M_\infty = 0.9$, it can be observed that the present results practically follow the same trend as those of XTRAN3S codes. Better correlations are found at lower frequencies than for those at higher frequencies. In Figure 5, overpredicted unsteady shock appears in section 5 which suggests that the three-dimensional, wave cancelling mechanism acts at high frequencies more effectively than a locally two-dimensional one. In Figure 7, the resulting unsteady pressures at $M_\infty = 0.95$ appear also to follow the same trend as those of NLR and XTRAN3S code, except that the unsteady shock strength is again overpredicted by the present method. To investigate this problem further, we change over the pressure input as predicted by XTRAN3S to the NLR measured data which contains a weaker mean shock. As shown in Figure 8, the unsteady pressures are indeed improved near the shock and are otherwise unaffected. This further verifies our contention that the steady shock strength and position are the most crucial for unsteady pressure predictions.

Figure 9 presents the in-phase and out-of-phase pressures of the LANN wing with pitching axis located at 62% root chord. Throughout five spanwise locations considered, the present results for upper-surface compare more favorably with the NLR measured data than do the XTRAN3S results. Meanwhile, subcritical flows are predicted for lower surfaces; hence, the unsteady pressures do not contain shock-jump. Figure 10 presents pressure results for a

highly-swept RAE tailplane of $\Lambda = 50.2°$ at $M_\infty = 0.9$ and at zero mean incidence. Because the present method uses the measured data inputs, it can be seen that the predicted unsteady shock positions correlate better with the RAE data than do the XTRAN3S results. It should be cautioned that Eq. (1) may not be suitable for wings with large sweepback angles, as the side wash could be of the same order as the mean convective velocity. One would therefore expect that for both steady and unsteady flow, discrepancies will occur near the wing tip, particularly for wings with low aspect ratios. Such deterioration in pressure estimates was observed in Ref. 9.

In general, overall trends of unsteady pressures were obtained with TES method from Figures 4 to 10. In some cases, insufficient adjustment of the phase angle causes the underprediction of the unsteady pressure level. It is believed that this type of discrepancy may result from the linear approximation inherent in the spanwise correction procedure.

Oscillating Flap

Figure 11 presents the computed and measured data at 45% semi-span of AGARD standard RAE wing with an oscillating flap starting at 70% chord. It is interesting to observe that the present results and Isogai's full potential method (Ref. 6) are in good agreement with RAE measured data. Figure 12 compares in- and out-of-phase pressures at two flap sections of F-5 wing at $M_\infty = 0.9$; the hinge line is located at 82% chord. Closed agreements are found with XTRAN3S results of Sotomayor and Borland (Ref. 8) and NLR measured data (Ref. 21). It should be pointed out that in presenting the flap oscillation data, usual practice in computational methods is to connect the data points across the hinge line, in the same manner as connecting the shock points; such are the cases of Refs. 6 and 8. However, control surface singularities in subsonic flow have been well established by White and Landahl (Ref. 22). Since the flow is assumed inviscid and is locally subsonic, hinge line singularity, as we have presented in these figures, should prevail.

Computation Time

In performing the first correction of the present TES code (LTRAN2/IAF2), we used typically 103 x 97 grid points and assigned 240 time steps for each cycle. Pressure data are read usually in the fourth cycle, as the aerodynamic response normally becomes periodic or harmonic after the third cycle. Typically, it takes 700 iterations to achieve the IAF2 steady pressure output. In an IBM 3081, the CPU time for the first correction amounts to some 620 seconds. With 10 x 10 panels, the Doublet Lattice code requires 40 seconds, with the additional procedure, the CPU time amounts to roughly 100 seconds. Hence, the total CPU time required for running TES code on one strip adds up to 720 seconds. The same case (e.g., Northrop F-5 wing) computed by XTRAN3S code would require reportedly 2000 to 4000 seconds CPU time in the CRAY-1S supercomputer. This would amount to an equivalent CPU time in an IBM 3081 of about 10 hours or more. With four strips chosen in this case, present TES method usually takes up no more than 3000 seconds. Therefore, a saving of about ten- to twelve-fold in CPU time can be achieved. With further improvement to the TES pilot code, it is expected that at least another reduction factor of two in CPU time can be achieved.

CONCLUDING REMARKS

A TES method has been developed for unsteady transonic computations about wing planforms. Four swept, tapered wings of various aspect ratios including control surfaces are selected as computational examples for validation of the TES computer code. Computed results of TES code practically follow the same trends as those of XTRAN3S codes and full-potential code; all of them have been verified with available measured data by NLR and RAE.

In view of the satisfactory results obtained and the effective procedures established by the TES method, we believe that it is useful for immediate aeroelastic applications. To summarize, the following special features of the TES method are worthy of notice:

Applicability to General Planforms

In addition to its applicability to rectangular wings, the TES method is equally applicable to swept and tapered wing planforms with any given aspect-ratio, including those with control surfaces.

No Need for Grid Generation

Any time-domain three dimensional computational methods generally requires a grid generation procedure, which could be planform-dependent in most cases. The present TES method does not require such a procedure.

Computation Efficiency

A rough estimate in CPU time indicates that to compute aerodynamics for one given mode, using the present TES method, is at least ten times faster than using the XTRAN3S code. With further improvement of the current TES pilot code, it is expected that at least another reduction factor of two in CPU time can be achieved.

Flexibility and Ease of Application

Unlike other unsteady computational methods, TES method makes use of the steady-flow pressures supplied either by measurement or by steady computational method. The flexibility of the TES method lies in the pressure input scheme which does not require airfoil shapes. For ease of application, the input format of TES code will be unified with that of the subsonic doublet lattice code.

Transonic A.I.C. and Flutter

With the exclusion of chordwise bending modes, the present TES method can be extended to the construction of a three-dimensional aerodynamic-influence-coefficient matrix, hence, the generalized forces. These are the essential building blocks for the TES method to become an efficient aerodynamic tool for flutter analysis.

REFERENCES

1. Ballhaus, W.F. and Goorjian, P.M., "Implicit Finite-Difference Computations of Unsteady Transonic Flows about Airfoils," AIAA Journal, Vol. 15, No. 12, December 1977, pp. 1728-1735.

2. Ballhaus, W.F. and Goorjian, P.M., "Computation of Unsteady Transonic Flows by the Indicial Method," AIAA Journal, Vol. 16, No. 2, February 1978, pp. 117-124.

3. Guruswamy, P. and Goorjian, P.M., "An Efficient Coordinate Transformation Technique for Unsteady Transonic Aerodynamic Analysis of Low-Aspect-Ratio Wings," AIAA Paper 84-0872-CP.

4. Borland, C.J. and Sotomayer, W.A., "An Algorithm for Unsteady Transonic Flow about Tapered Wings," AIAA Paper 84-1567.

5. Edwards, C.J., Bland, S.R. and Seidel, D.A., "Experience with Transonic Unsteady Aerodynamic Calculations," NASA TM 86278, August 1984.

6. Isogai, K. and Suetsugu, K., "Numerical Calculations of Unsteady Transonic Potential Flow Over Three-Dimensional Wings with Oscillating Control Surfaces," AIAA Journal, Vol. 22, No. 4, April 1984, pp. 478-485.

7. Malone, J.B. and Ruo, S.Y., "Computation of Unsteady Transonic Flows about Two-Dimensional and Three-Dimensional AGARD Standard Configurations," AGARD Specialist Meeting on Transonic Unsteady Aerodynamics and Its Aeroelastic Applications, Toulouse, France, September 3-6, 1984.

8. Sotomayer, W.A. and Borland, C.J., "Numerical Computation of Unsteady Transonic Flow about Wings and Flaps," AIAA Paper 85-1712.

9. Bennett, R.M., Wynne, E.C. and Mabey, D.G., "Calculations of Transonic Steady and Oscillatory Pressures on A Low Aspect Ratio Model and Comparison with Experiment," Paper 85-17, 2nd International Symposium on Aeroelasticity and Structural Dynamics, Aachen, Germany, April 1-3, 1985.

10. Malone, J.B. and Ruo, S.Y., "LANN Wing Test Program: Acquisition and Application of Unsteady Transonic Data for Evaluation of Three-Dimenssional Computational Methods," AFWAL-TR-83-3006, February 1983.

11. Liu, D.D., "Computational Transonic Equivalent Strip Method for Applications to Unsteady 3D Aerodynamics," AIAA Paper 83-0261.

12. Couston, M., Angelini, J.J. and Meurzec, J.P., "Comparison des Champs de Pression Instationnaire Calcules et Mesure sur le Modele ZKP," AGARD-R-688, April 1980, pp. 1-1 to 1-16.

13. Zwann, R.J., "Verifications of Calculation Methods for Unsteady Airloads in the Prediction of Transonic Flutter," AIAA Paper 84-0871.

14. Fung, K.Y. and Chung, A., "Computations of Unsteady Transonic Aerodynamics Using Prescribed Steady Pressures," Journal of Aircraft, Vol. 20, No. 12, December 1983, pp. 1058-1061.

15. Rodden, W.P., Giesing, J.P. and Kalman, T.P., "New Developments and Applications of the Subsonic Doublet Lattice Method for Nonplanar Configurations," AGARD Symposium on Unsteady Aerodynamics for Aeroelastic Analyses of Interfering Surfaces, Paper No. 4, May 1970.

16. Fung, K.Y., "A Simple, Accurate and Efficient Algorithm for Unsteady Transonic Flow," Recent Advances in Numerical Methods in Fluid Dynamics, W.G. Habashi, Ed., Pineridge Press, Swansea, U.K., 1984.

17. Lambourne, N.C., "Experimental Techniques in Unsteady Aerodynamics," AGARD Report No. 679, Special Course on Unsteady Aerodynamics, June 18, 1980, pp. 10-1 to 10-26.

18. Horsten, J.J., Den Boer, R.G. and Zwaan, R.J., "Unsteady Transonic Pressure Measurements on a Semi-Span Wing Tunnel Model of a Transport-Type Supercritical Wing (LANN Model)," NLR TR-82-069U, Parts I and II and AFWAL-TR-83-3039, Part I and II, March 1983.

19. Tijdeman et al., "Transonic Wing Tunnel Tests on an Oscillating With with External Store, Part II: The Clean Wing," NLR TR 78106U, Part II, also AFFD; -TR-78-194, January 1978.

20. Mabey, D.G., McOwat, D.M. and Welsh, B.L., "Aerodyanamic Characteristics of Moving Trailing-Edge Control at Subsonic and Transonic Speeds," Aerodynamic Characteristics of Controls, AGARD-CP-262, May 1982, pp. 20-1 to 20-25.

21. Persoon, A.J., Roos, R. and Schippers, P., "Transonic and Low Supersonic Wind-Tunnel Tests on a Wing with Inboard Control Surface," AFWAL-TR-80-3146, December 1980.

22. White, R.B. and Landahl, M.T., "Effect of Gaps on the Loading Distribution of Planar Lifting Surfaces," AIAA Journal, Vol. 6, No. 4, April 1968, pp. 626-631.
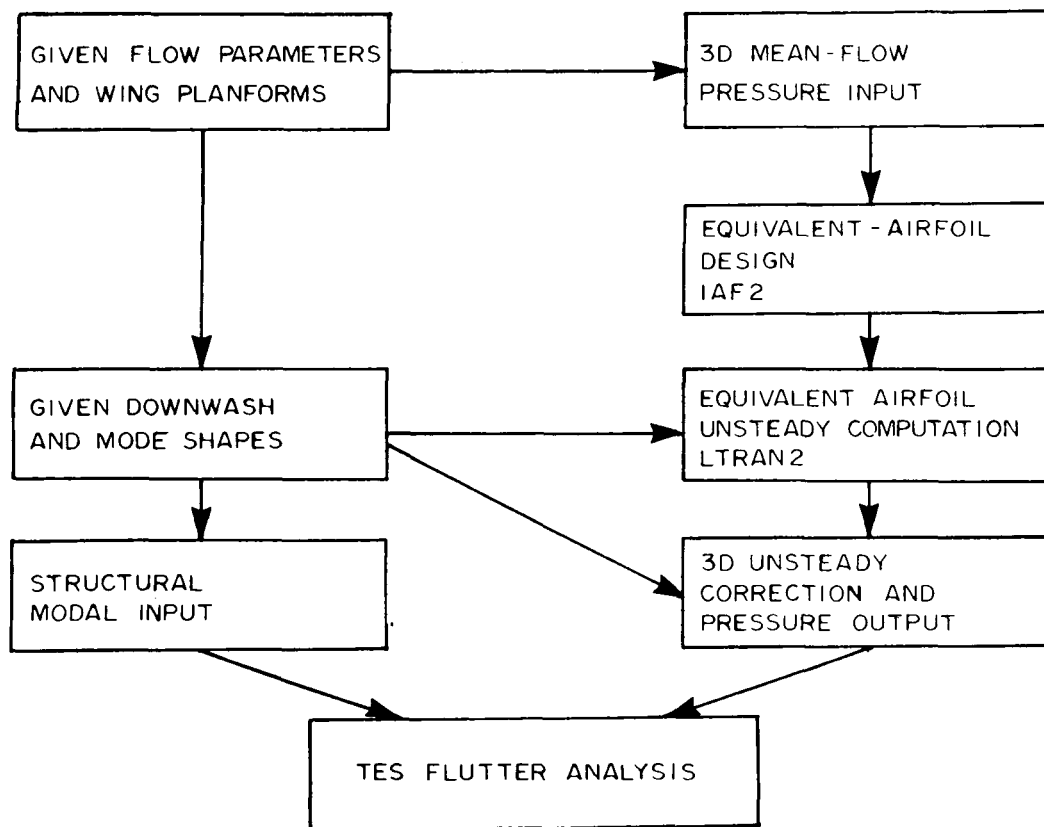
Fig. 1 Flow Chart Showing TES Computation Procedure

$$R_1 = \sqrt{(\lambda a_\infty \bar{t})^2 - (\lambda \bar{y}_0)^2}$$

$$R_2 = \sqrt{(\lambda a_\infty \bar{t})^2 - (\bar{x}_0 - U_\infty \bar{t})^2}$$

(A)

(B)
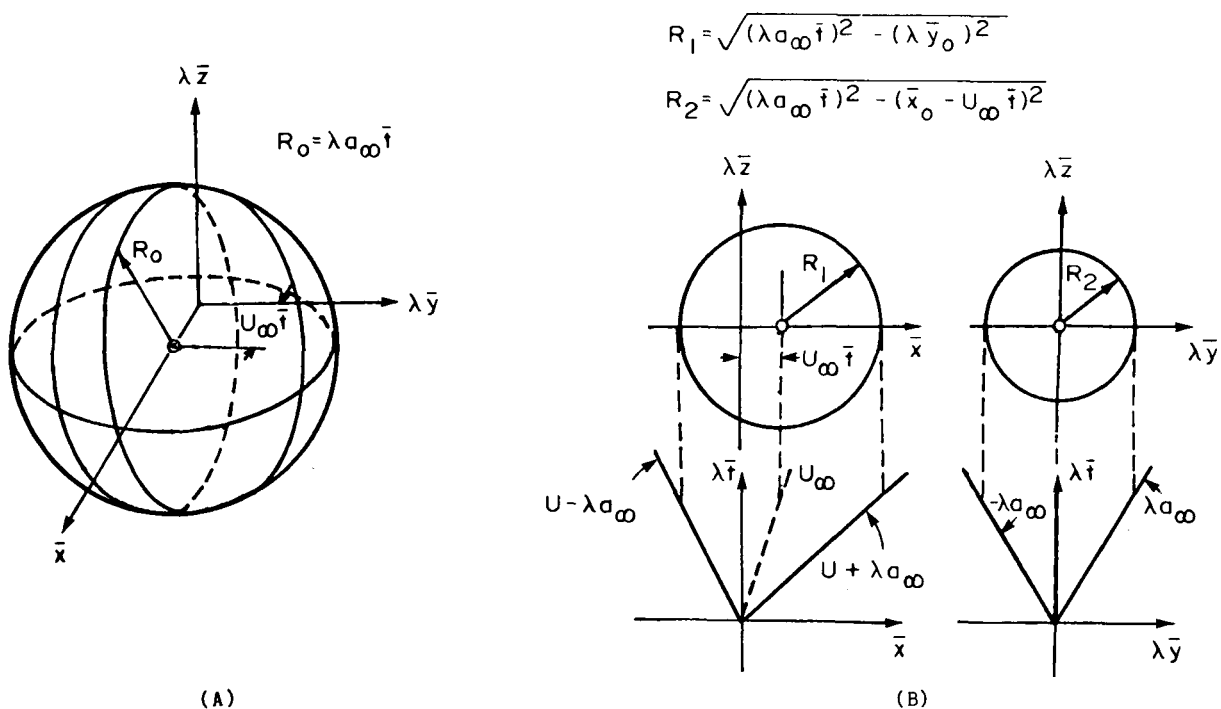
Fig. 2 (A) Characteristic Sphere
(B) Wave Propagations in Strip Planes

146

(A) LANN WING
M_∞ = 0.82

(B) NORTHROP F-5 WING
M_∞ = 0.90

(C) NORTHROP F-5 WING
M_∞ = 0.95
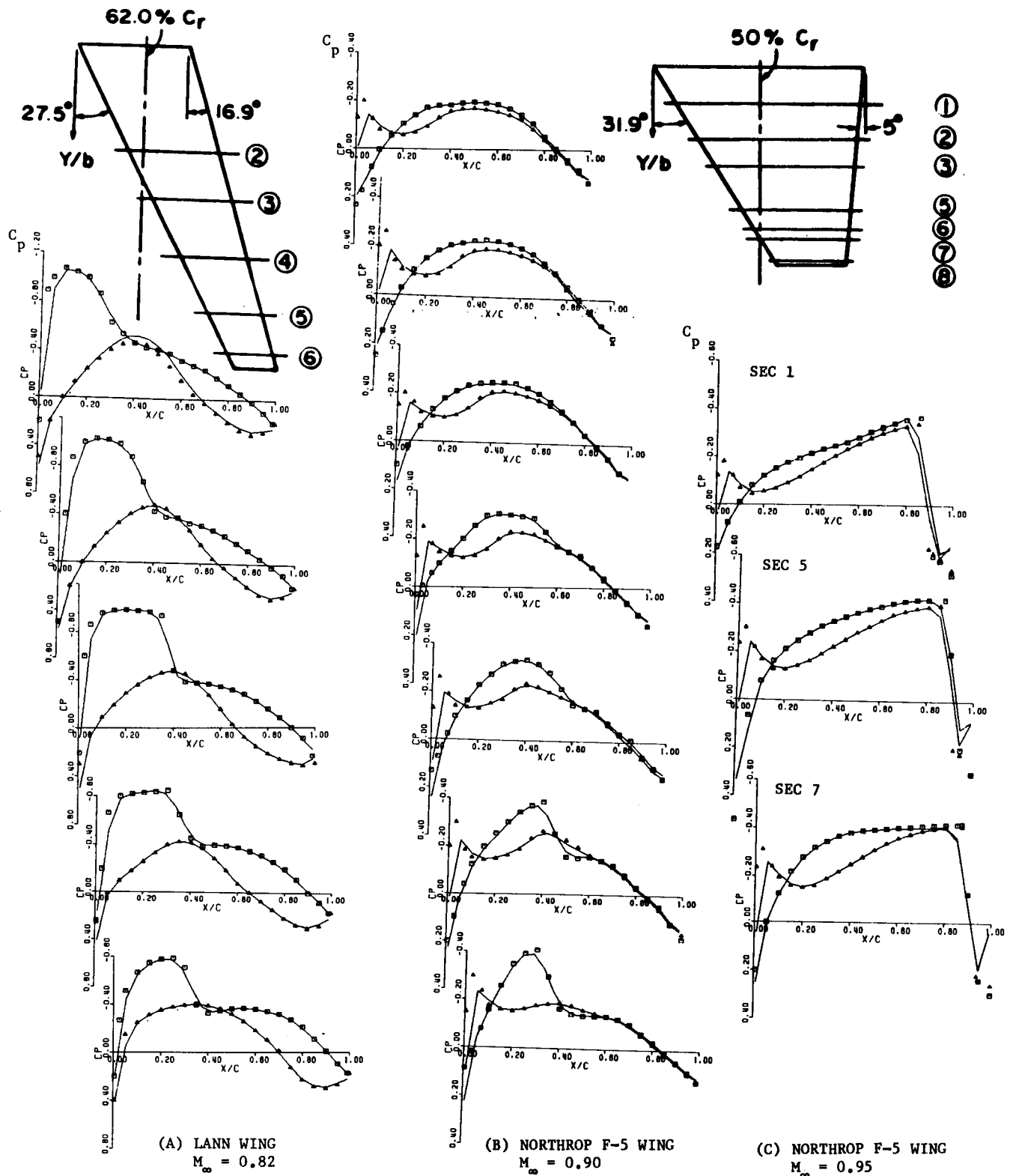
Fig. 3   Steady Pressure Inputs and Equivalent-Airfoil Outputs at Various Spanwise Locations for:
(A)   LANN WING at Mean Incidence α_0 = 0.62°
(B) and (C)   NORTHROP F-5 WING at Mean Incidence α_0 = 0°
(▣ Upper and △ Lower Surfaces - Measured Data: (A) NLR/Horsten, (B) NLR/Tijdeman and
(C) Computed Data XTRAN3S/Ames; ————— Present Equivalent-Airfoil Output)
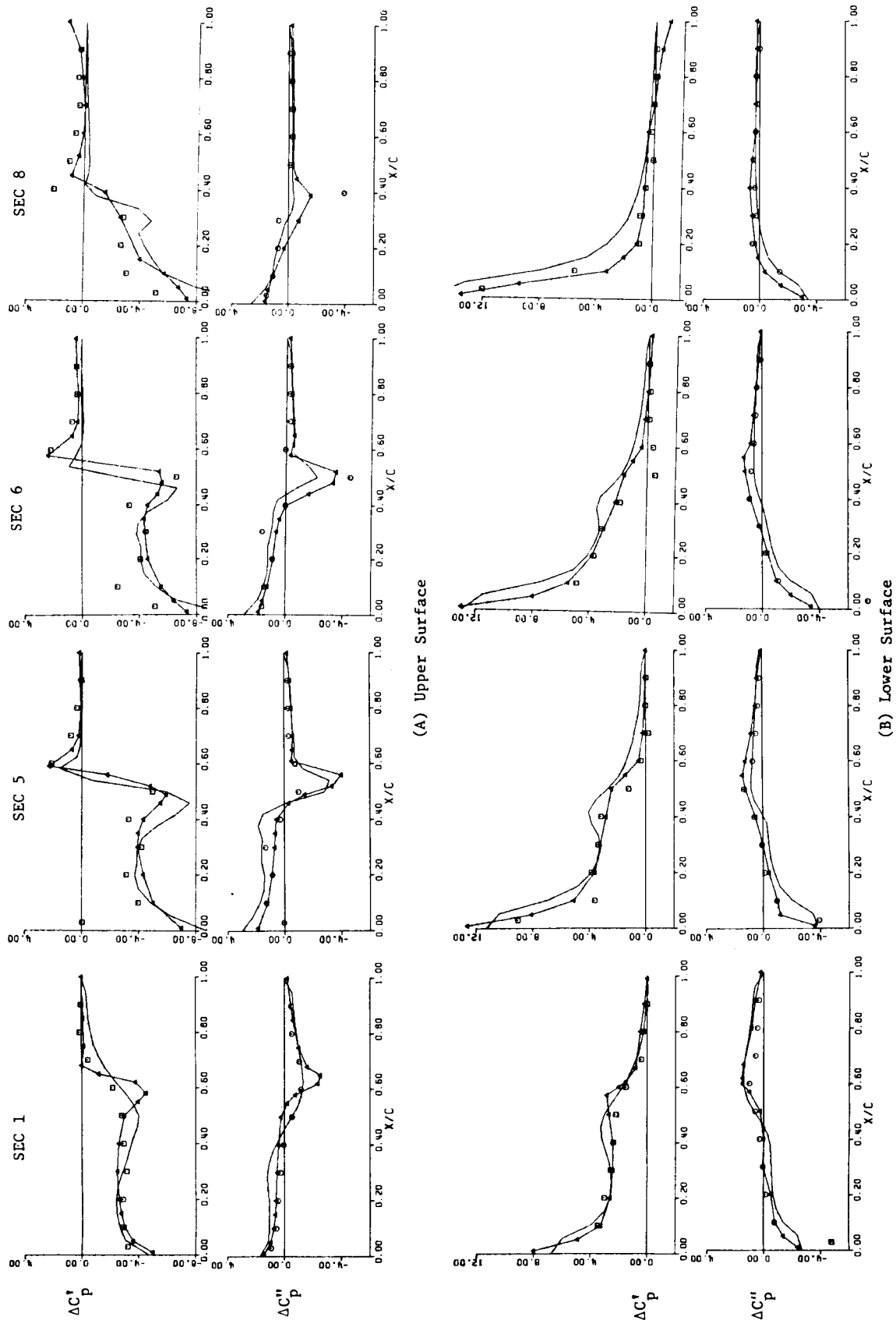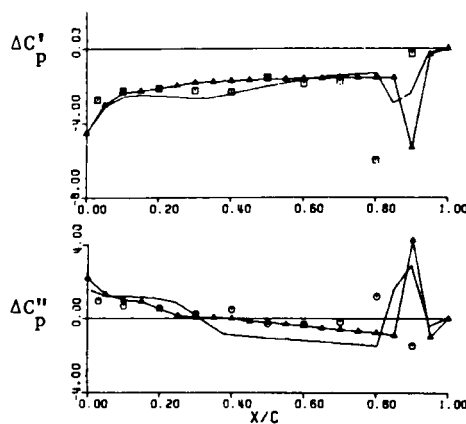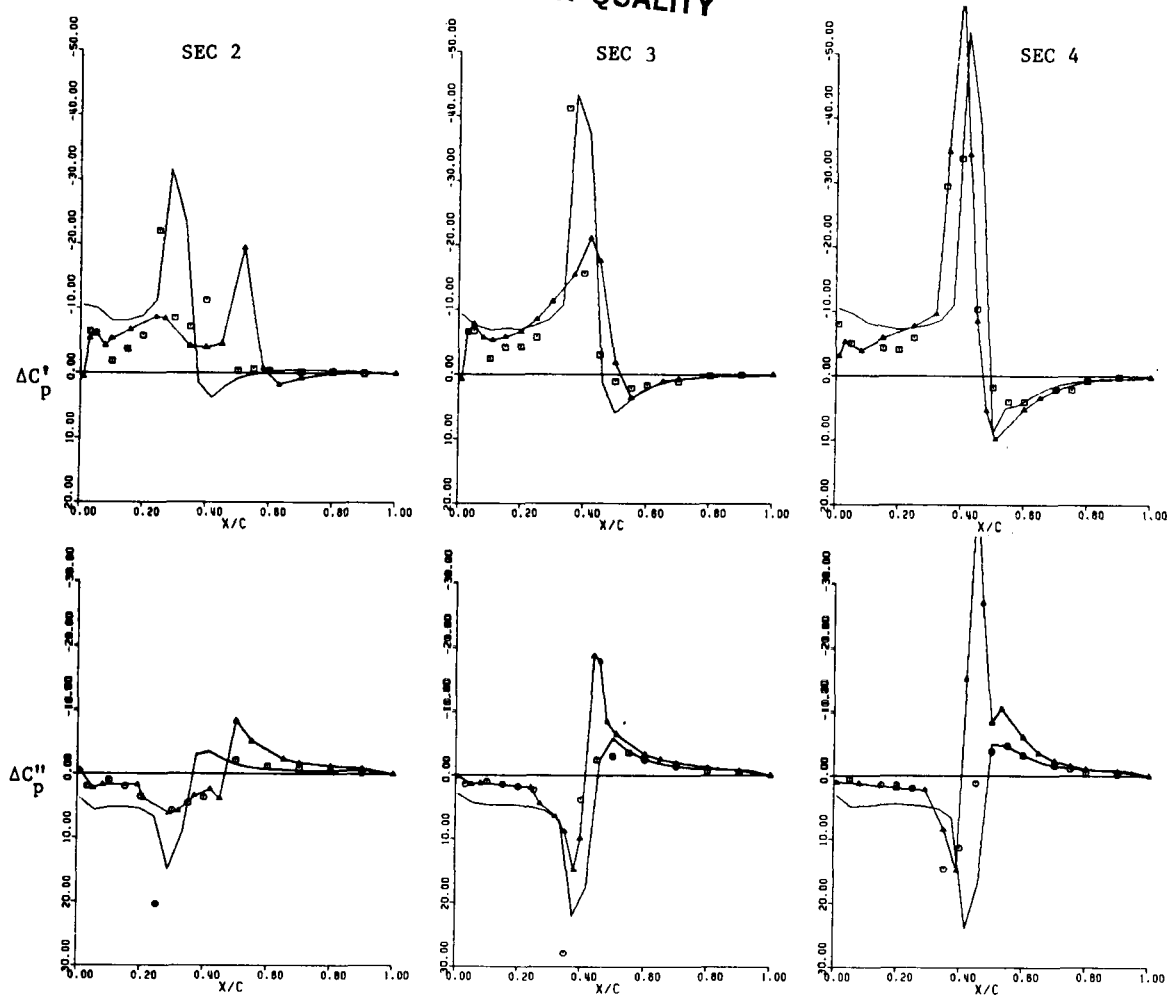
Fig. 4 NORTHROP F-5 WING Comparison of In-phase and Out-of-phase Pressures at Four Spanwise Locations: Pitching Oscillation about Mid Root-Chord at Mach Number $M_\infty = 0.90$ and Reduced Frequency $k = 0.274$. (—— Present TES Method; —△— XTRAN3S/Borland et al.; □ Real and ⊙ Imaginary - NLR/Tijdeman et al. Measured Data)

148
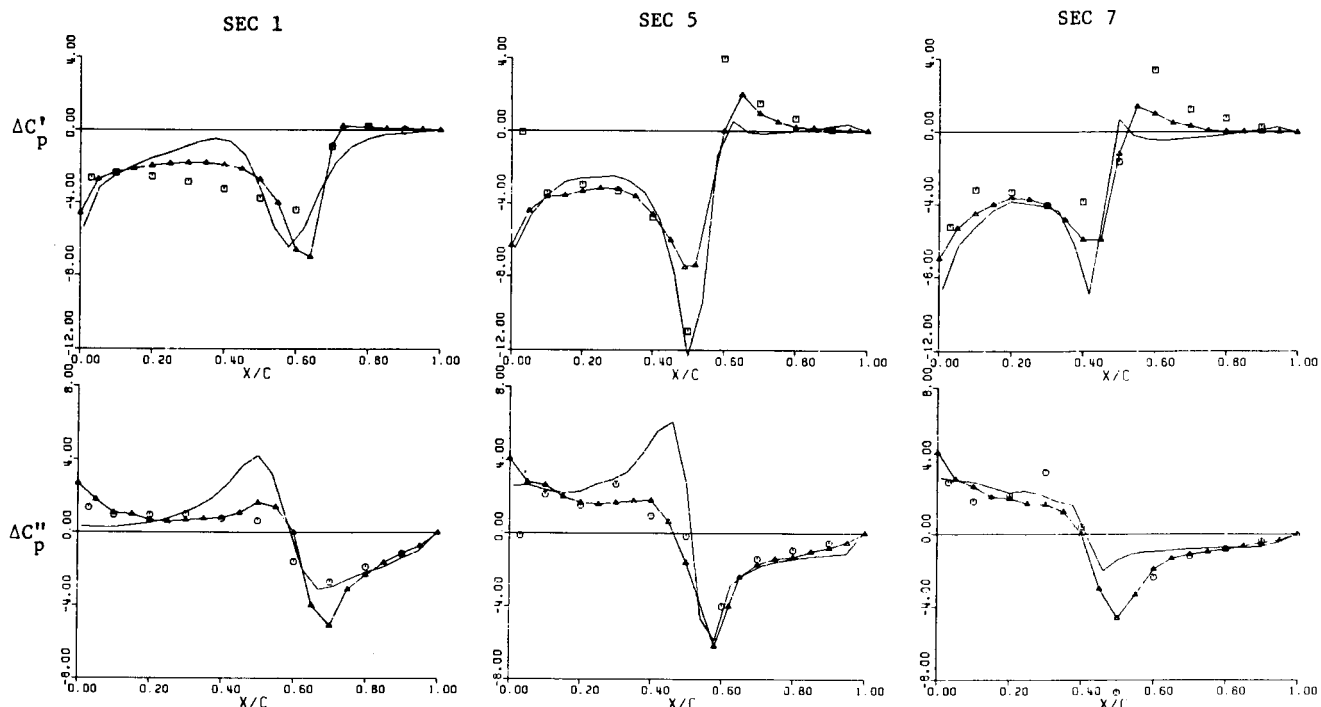
Fig. 5 NORTHROP F-5 WING Comparison of In-phase and Out-of-phase Pressures on Upper Surface at Three
Spanwise Locations: Pitching Oscillation about Mid Root-Chord at Mach Number M_∞ = 0.90 and
Reduced Frequency k_c = 0.550.
(———— Present TES Method; ——△—— XTRAN3S/Ames; ⊡ Real and ⊙ Imaginary - NLR/Tijdeman et al.
Measured Data)
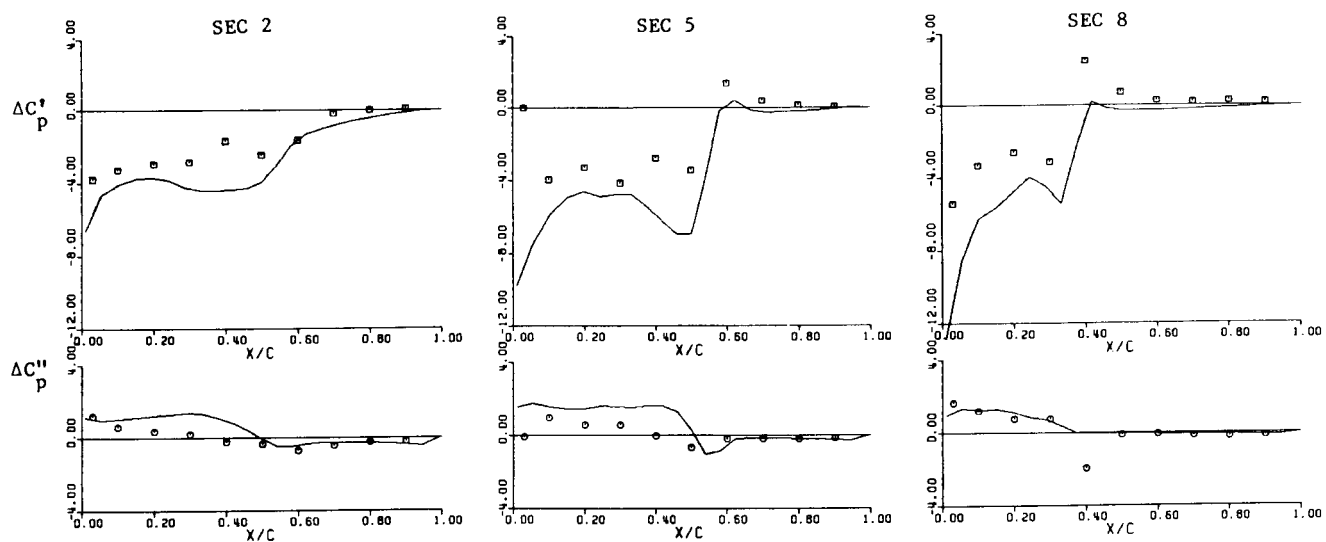
Fig. 6 NORTHROP F-5 WING Comparison of In-phase and Out-of-phase Pressures on Upper Surface at Three
Spanwise Locations: Pitching Oscillation about Mid Root-Chord at Mach Number M_∞ = 0.90 and
Reduced Frequency k_c = 0.136.
(————Present TES Method; ⊡ Real and ⊙ Imaginary - NLR/Tijdeman et al. Measured Data)

149
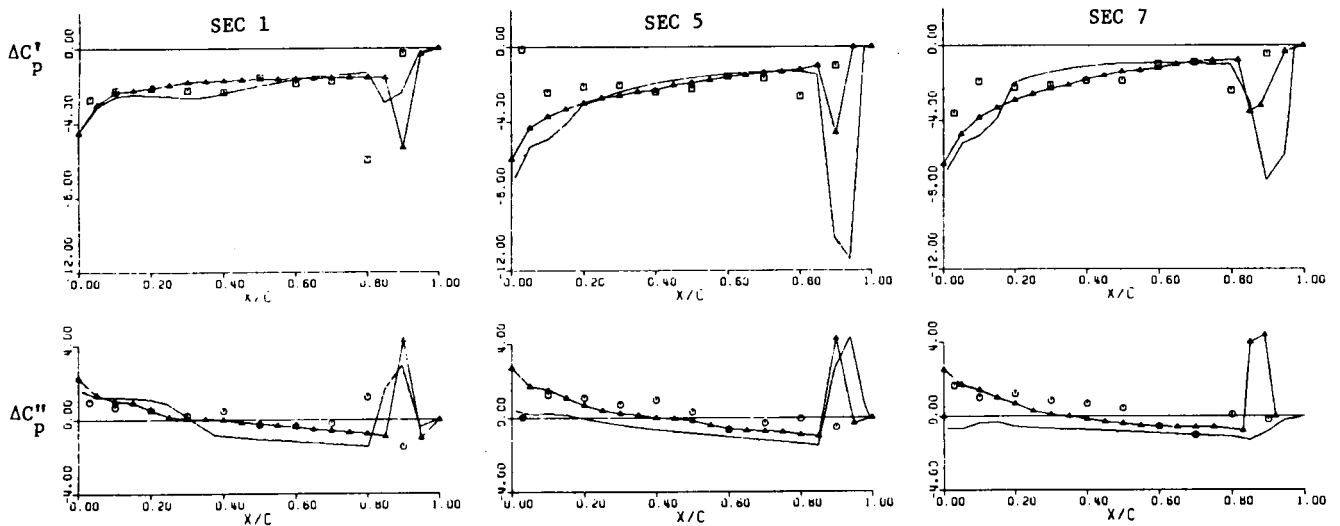
Fig. 7   NORTHROP F-5 WING   Comparison of In-phase and Out-of-phase Pressures on Upper Surface at Three
Spanwise Locations: Pitching Oscillation about Mid Root-Chord at Mach Number $M_\infty = 0.95$ and
Reduced Frequency $k_c = 0.528$.
(——— Present TES Method; —△— XTRAN3S/Ames; ▣ Real and ⊙ Imaginary - NLR/Tijdeman et al.
Measured Data)
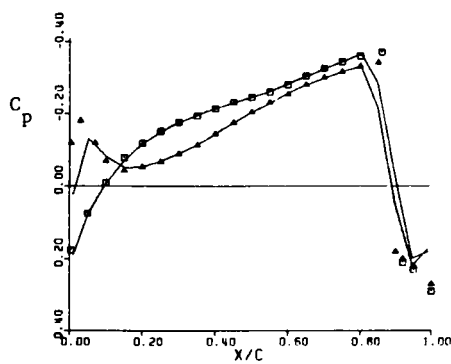
(A) XTRAN3S/Ames Input
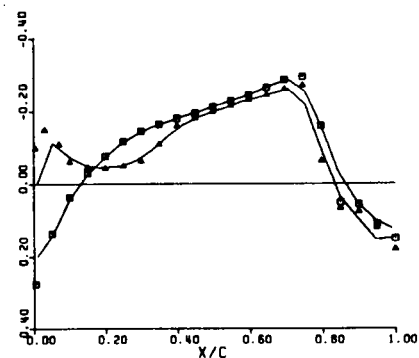
(B) NLR Measured Data Input
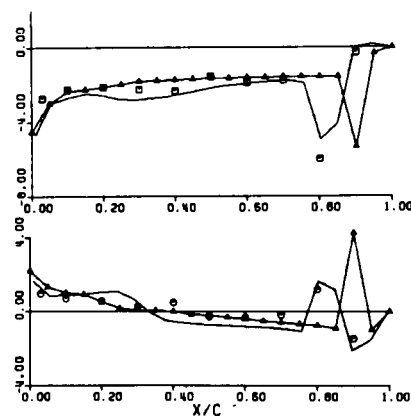
Fig. 8   NORTHROP F-5 WING   Comparison of Steady Pressure Distributions, In-phase and Out-of-phase
Pressures at 18% Spanwise Locations: Pitching Oscillation about Mid Root-Chord at Mach Number
$M_\infty = 0.95$ and Reduced Frequency $k_c = 0.528$.
(——— Present TES Method; —△— XTRAN3S/Ames; ▣ Real and ⊙ Imaginary - NLR/Tijdeman et al.
Measured Data)

150

SEC 2   SEC 3   SEC 4

$\Delta C_p'$

$\Delta C_p''$

(A) LANN WING   Upper Surface
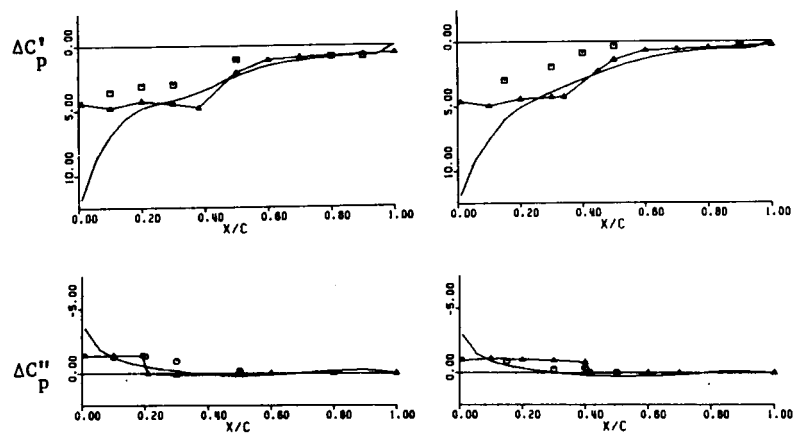
$\Delta C_p'$

$\Delta C_p''$
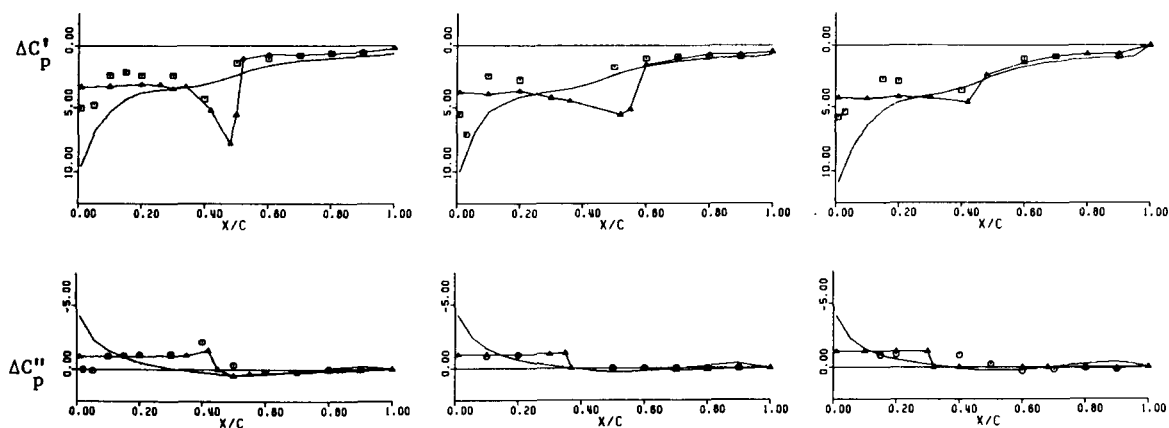
(B) LANN WING   Lower Surface

Fig. 9   LANN WING   Comparison of In-phase and Out-of-phase Pressures at Five Spanwise Locations :
Pitching Oscillation about 62% Root-Chord at Mach Number M_∞ = 0.82 and Reduced Frequency
k_c = 0.205
(———— Present TES Method; —△— XTRAN3S/Malone; ▢ Real and ⊙ Imaginary - NLR/Horsten et al.
Measured Data)

151
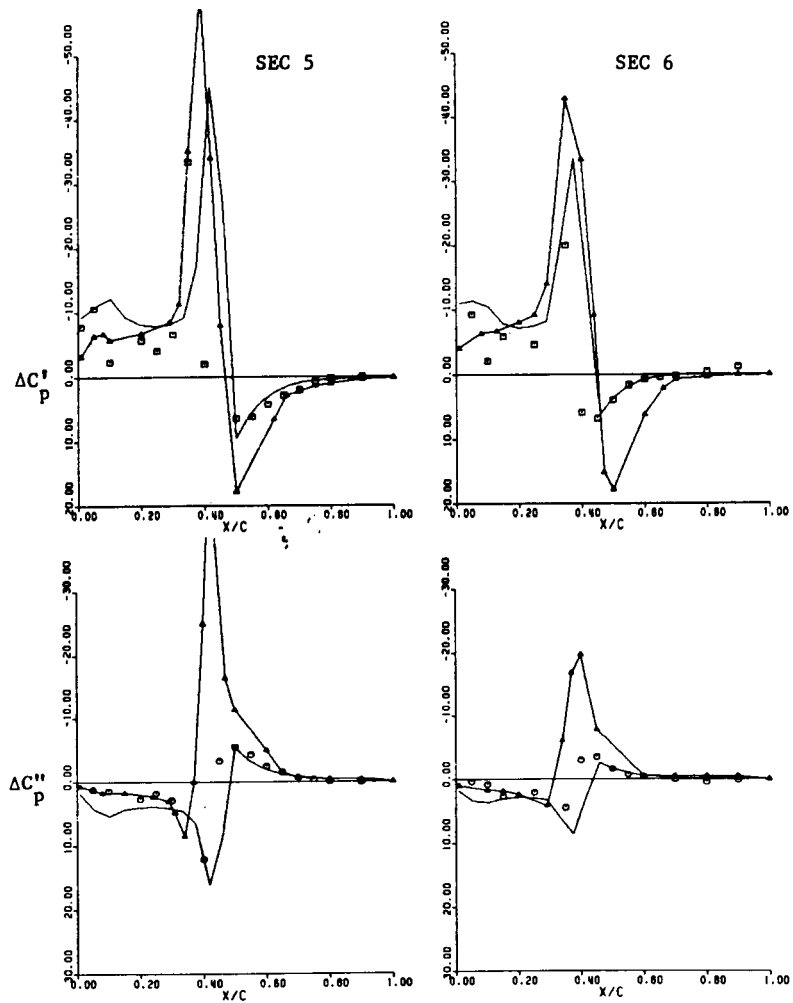
(A) LANN WING Upper Surface [Continued]

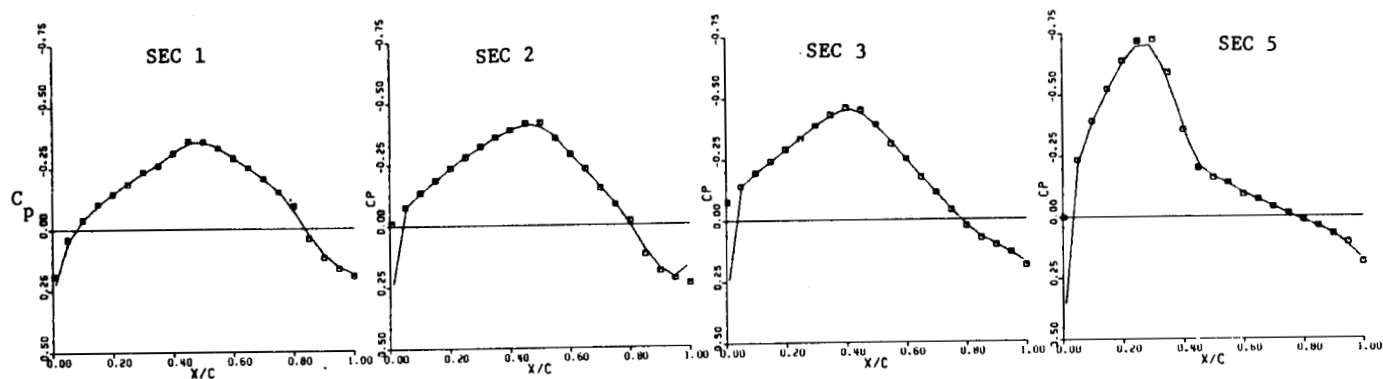(B) LANN WING Lower Surface [Continued]

Fig. 9 LANN WING [Continued]

Y/b

$\Lambda = 50.2°$

① ② ③ ⑤
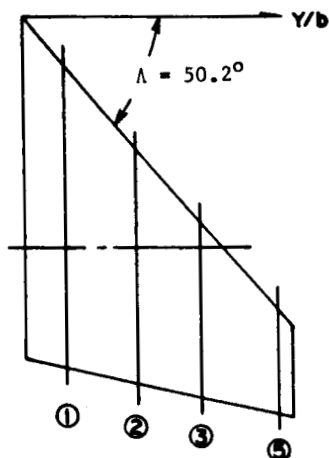
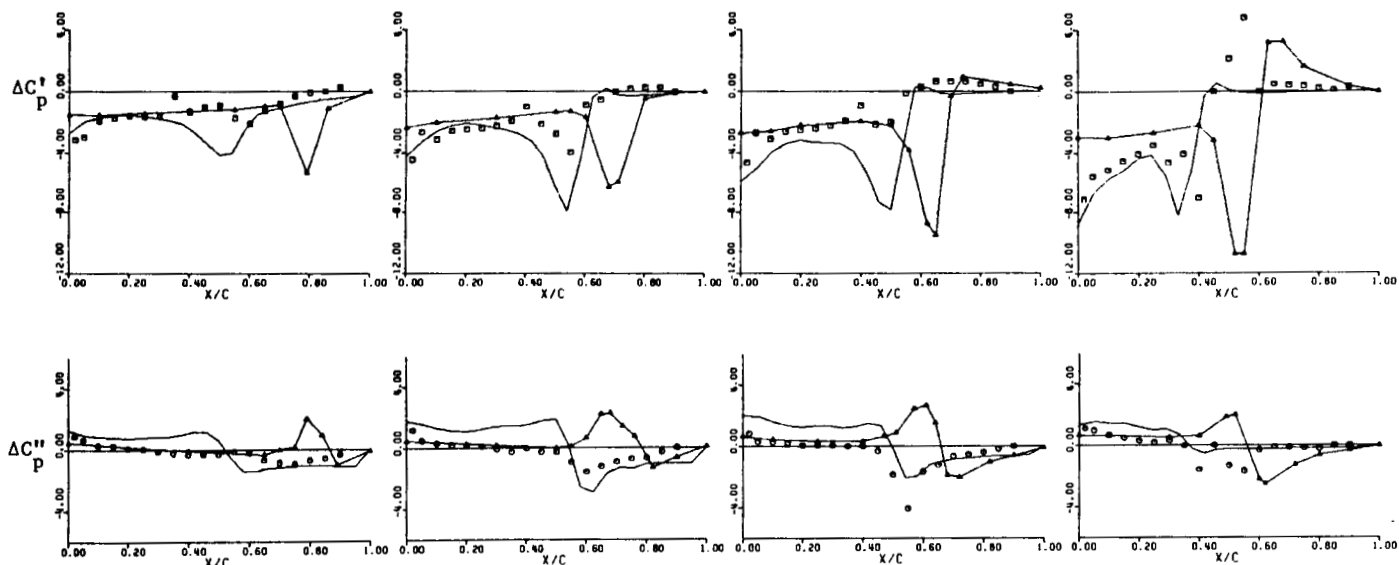RAE AGARD TAILPLANE:
ASPECT RATIO   : AR=2.41
TAPER RATIO   : TR=0.27
MACH NUMBER   : M_∞=0.90
MEAN INCIDENCE   : α_0=0°
REDUCED FREQUENCY: k_c=0.422
PITCHING AXIS   : x_0=68.2% ROOT CHORD
OSCILLATION AMPLITUDE: α_1=0.4°

SEC 1   SEC 2   SEC 3   SEC 5

(A) Steady Pressure Distributions

(B) In-phase and Out-of-phase Pressures

Fig. 10 RAE AGARD TAILPLANE:
(A) Steady Pressure Inputs and Equivalent-Airfoil Pressure Outputs at Four Spanwise Locations
(▣ RAE Measured Data Input; ——— Equivalent-Airfoil Output)
(B) Comparison of In-phase and Out-of-phase Pressures
(——— Present TES Method; —△— XTRAN3S/Bennett et al.; ▣ Real and ⊙ Imaginary
-RAE Measured Data)

153

X/C = 0.70

(A) Steady Pressure Distribution
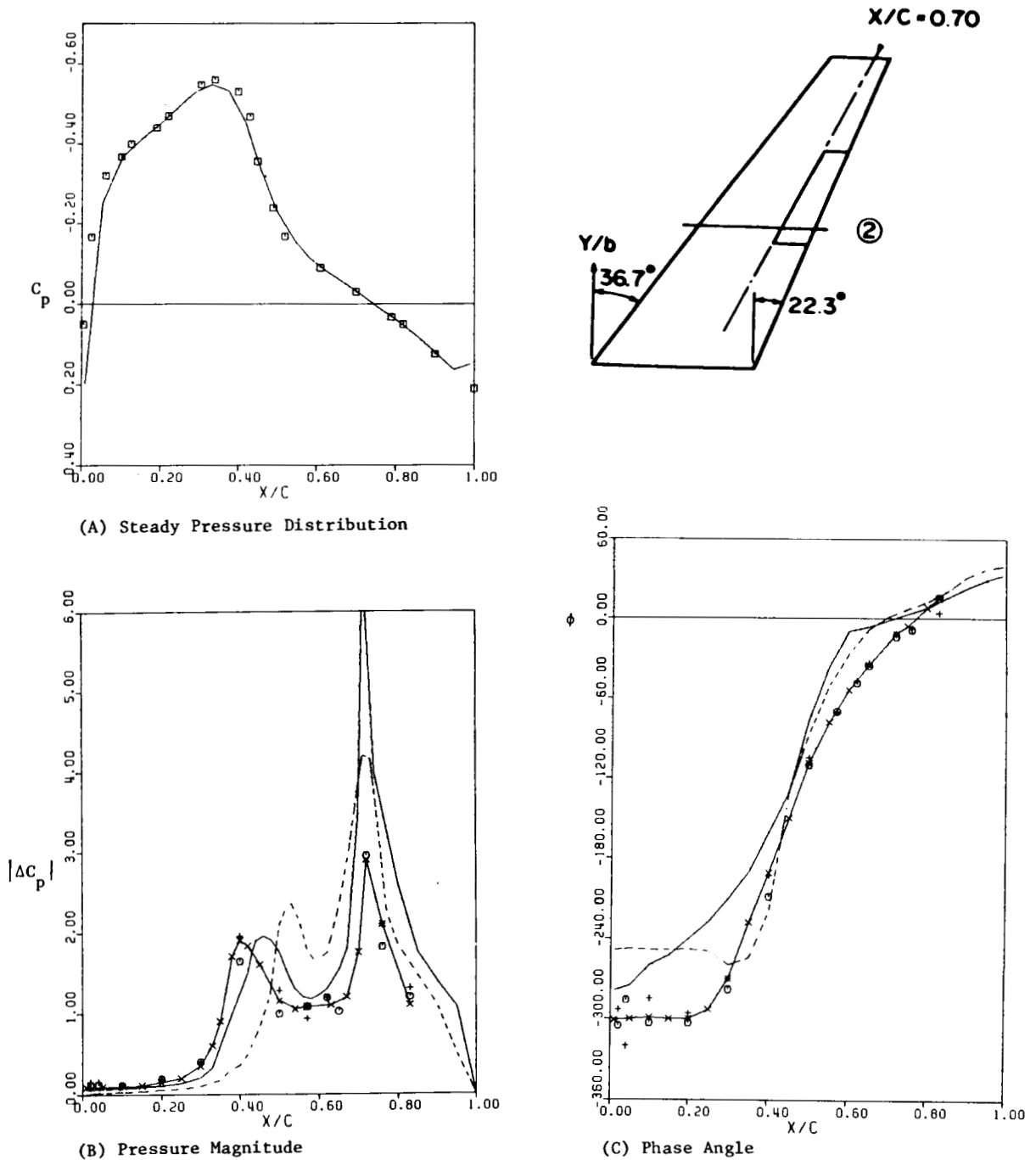
Y/b
36.7°
22.3°
②

(B) Pressure Magnitude

(C) Phase Angle

Fig. 11 AGARD STANDARD RAE WING WITH OSCILLATING FLAP
(A) Steady Pressure Inputs and Equivalent-Airfoil Pressure Outputs at 45% Spanwise Location at
Mach Number M_∞ = 0.90 and Mean Incidence α_o = 0°
(☐ GACBOPPE Code Input; ——— Equivalent-Airfoil Output)
(B) Pressure Magnitude and
(C) Phase Angle on Upper Surface of 45% Spanwise Location for AGARD RAE Wing with Oscillating
Flap at Mach Number M_∞ = 0.90 and Reduced Frequency k_c = 0.705 with Flap Amplitude δ = 1°
(——— Present TES Method; ------Isogai's Full Potential Code; O + ✳ RAE Measured Data)

(A) 18% Spanwise Location (Section 1)
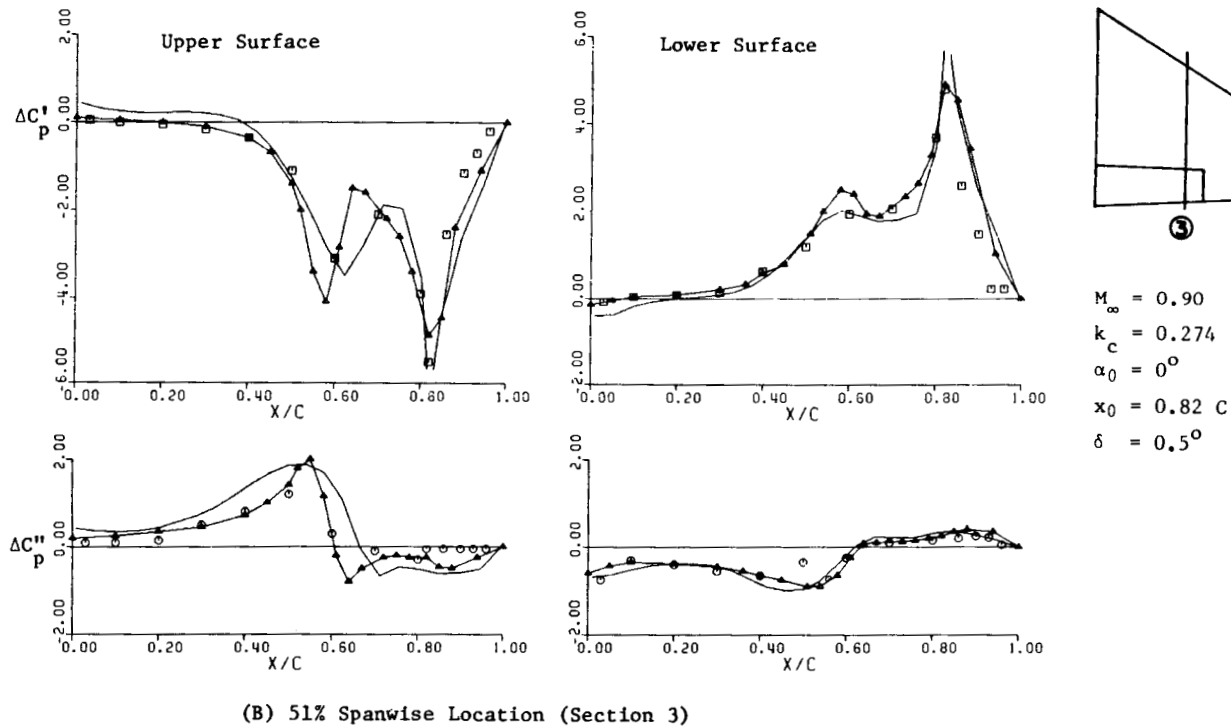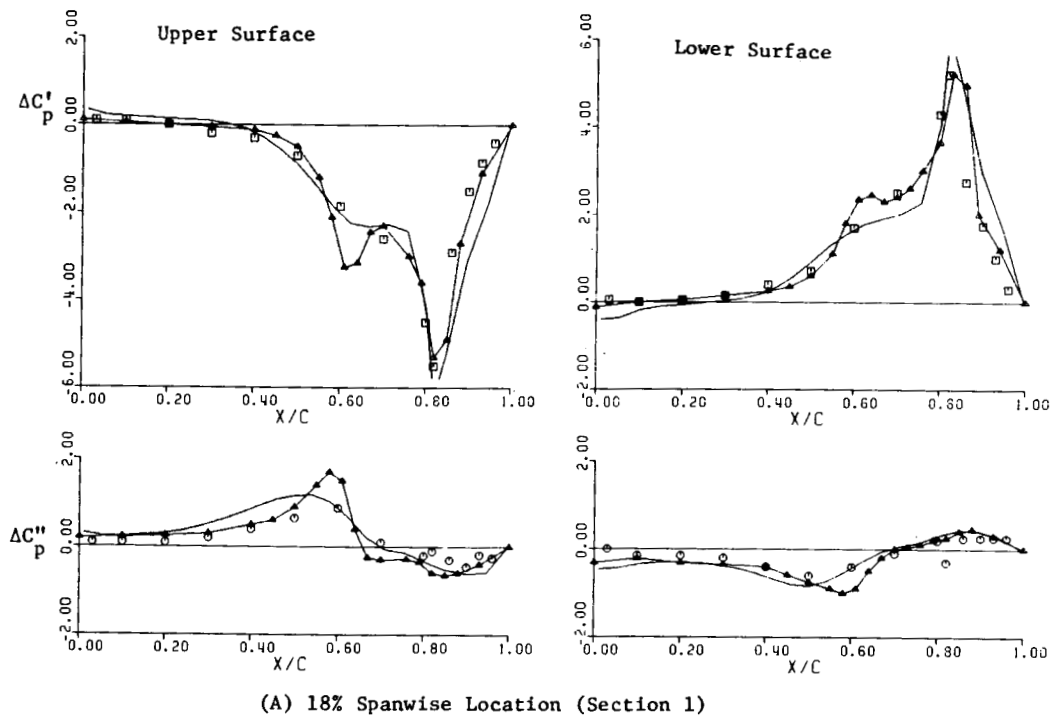
(B) 51% Spanwise Location (Section 3)

Fig. 12 NORTHROP F-5 WING WITH OSCILLATING FLAP
Comparison of In-phase and Out-of-phase Pressures with Hinge Line at 82% Chord at
Sections 1 and 3.
(——— Present TES Method; —△— XTRAN3S/Sotomeyer; ⊡ Real and ⊙ Imaginary
- NLR/Tijdeman et al. Measured Data)